2024-11-01

Confocal Raman Spectroscopy Coupled With in Vitro Permeation Testing to Study the Effects of Formalin Fixation on the Skin Barrier Function of Reconstructed Human Epidermis

Hichem Kichou
UPR CNRS 4301 CBM, département NMNS « NanoMédicaments et NanoSondes », Université de Tours, 31 avenue Monge, 37200 Tours.

Franck Bonnier
LVMH Recherche, 185 Av. de Verdun, 45800, Saint-Jean-de-Braye, France.

Amanda C. Caritá
FOCAS Research Institute, TU Dublin, City Campus, Camden Row, Dublin 8, D08 CKP1, Ireland

See next page for additional authors

Confocal Raman spectroscopy coupled with *in vitro* permeation testing to study the effects of formalin fixation on the skin barrier function of reconstructed human epidermis

Hichem Kichou [a], Franck Bonnier [b], Amanda C. Caritá [a], Hugh J. Byrne [c], Igor Chourpa [a] and Emilie Munnier [a*]

[a] UPR CNRS 4301 CBM, département NMNS « NanoMédicaments et NanoSondes », Université de Tours, 31 avenue Monge, 37200 Tours.

[b] LVMH Recherche, 185 Av. de Verdun, 45800, Saint-Jean-de-Braye, France.

[c] FOCAS Research Institute, TU Dublin, City Campus, Camden Row, Dublin 8, D08 CKP1, Ireland.

*corresponding author: Emilie Munnier, UPR CNRS 4301 CBM, département NMNS « NanoMédicaments et NanoSondes », Université de Tours, 31 avenue Monge, 37200, France; Tel: +33 2 47367307; E-mail: emilie.munnier@univ-tours.fr

Abstract:

Confocal Raman Spectroscopy is recognised as a potent tool for molecular characterisation of biological specimens. There is a growing demand for *In Vitro* Permeation Tests (IVPT) in the pharmaceutical and cosmetic areas, increasingly conducted using Reconstructed Human Epidermis (RHE) skin models. In this study, chemical fixation of RHE in 10% Neutral Buffered Formalin for 24 hours has been examined for storing RHE samples at 4°C for up to 21 days. Confocal Raman Spectroscopy, combined with Principal Components Analysis, revealed the molecular-level effects of fixation, notably in protein and lipid conformation within the *stratum corneum* and viable epidermis. IVPT by means of high-performance liquid chromatography, using caffeine as a model compound, showed minimal impact of formalin fixation on the cumulative amount, flux, and permeability coefficient after 12 hours. While the biochemical architecture is altered, the function of the model as a barrier to maintain rate-limiting diffusion of active molecules within skin layers remains intact. This study opens avenues for enhanced flexibility and utility in skin model research, promising insights into mitigating the limited shelf life of RHE models by preserving performance in fixed samples for up to 21 days.

Keywords: Confocal Raman Spectroscopy, Principal Component Analysis, *In Vitro* Permeation Test, Reconstructed Human Epidermis, Formalin fixation, samples storage.

Introduction

Skin is the largest organ of the human body, acting as a barrier, from the inside out, to prevent excessive trans epidermal loss of body water, but also from the outside in, to protect against external physical, chemical, and biological aggressions [1]. The specific biochemical architecture of the *stratum corneum* (SC), described as “bricks and mortar” [2], provides this efficient barrier function [3], that limits the permeability of the skin to exogenous agents, including to Active Cosmetic and Pharmaceutic Ingredients (ACI/API) released from topically applied formulations.

Since the 1990s, Confocal Raman Spectroscopy (CRS) has been applied to analyse skin. Early studies enabled the identification of spectral features in the biomolecular components of the *Stratum Corneum (SC)* in post-mortem skin samples [4, 5]. In 1998, Caspers et al., performed a similar CRS analysis of excised human skin sections, confirming that, while the dermis is dominated by signatures of collagen, the *SC* is dominated by contributions from keratin and lipids [6]. Notably, the study also demonstrated that CRS could be used for depth profiling, or "optical sectioning," of the biochemical composition of the skin, opening up new prospects for non-invasive, *in situ* / *in vivo* monitoring of dermatological processes [6].

Today, CRS is well-established as a powerful tool that can be utilised as a chemical characterisation tool to collect information about skin composition [7–10]. Many studies reported in the literature have demonstrated the suitability of the technique to investigate physiological processes such as cell and tissue maturation [11], serving as an imaging tool coupled to multivariate analysis for the diagnosis of skin pathologies [12, 13]. This includes the comparison of *ex vivo* / *in vitro* skin models [14, 15], and the study of the effects of exogenous agents such as UV radiation [16, 17]. CRS can also be employed to monitor the *in vitro* penetration and permeation of Active Pharmaceutical or Cosmetic Ingredient (API / ACI) [18–20]. More recently, CRS has been extensively explored to analyse human skin *in vivo*, studying hydration and the effects of Natural Moisturising Factors (NMF) [21, 22], monitoring penetration enhancers in the SC [23], tracking phospholipid permeation into the skin [24], and delivering active ingredients to *in vivo* skin [25].

Since the 1980s, fixation methods have been developed to capture a 'snapshot' of biological materials, allowing for morphological or histological investigations under conditions closely resembling *in vivo* situations [26]. Vibrational spectroscopy has been recognized as a valuable molecular characterisation tool for examining and characterising modifications in biochemical signatures induced by various fixation procedures at both cellular and tissue levels.

At the cellular level, several studies have explored the impact of fixative agents in pre-analytical protocols designed to prepare individual cells for microscopic investigation. Comparing the effects of fixation on C-3-prostate cancer cell line by formalin and glutaraldehyde, Gazi et al., used Synchrotron Radiation-Fourier Transformed Infrared spectroscopy to demonstrate that formalin at low concentration preserved the lipids, phosphate and protein content without impacting significantly the spectrum of the cells [7]. Similarly, Meade et al., concluded that, in comparison to Carnoy's fixative and a methanol-glacial-acetic mixture, formalin fixation resulted in Raman spectral signatures which were closest to those of live skin, bronchial epithelium and lung adenocarcinoma cells, and consequently, it best preserved their cellular integrity [27]. Draux et al. employed Raman imaging on individual cancer cells, revealing that formalin-fixation and cytocentrifugation have negligible effects on biochemical information when compared to living conditions [28]. It was later confirmed by Dorney et al. that the fixation of lung adenocarcinoma cell line (A549) by formalin improved sample stability during analysis, while it had negligible effects on Raman spectral features compared to live cells [29]. In 2015, Farhane et al. demonstrated that fixation of cells using formalin did not show any effect on the cells, and the discrimination between normal and cancerous cell lines *in vitro* based on the Raman spectra was not impacted [8]. Additionally, in 2017, Hobro and Smith illustrated, through Raman imaging on wild-type mouse embryonic fibroblasts, that aldehyde fixation methods are more suitable for studies that prioritize overall molecular content, aiming to closely mimic living conditions [30]. These studies conducted on different cell lines indicate that the fixation of biological materials can be achieved with minimal effects at the biomolecular level.

At tissue level, the standard procedure for preparing histopathological samples involves several steps. Firstly, tissue samples are fixed; secondly, they are embedded in paraffin, forming solid wax 'blocks'; thirdly, thin slices are sectioned using a microtome; finally, the tissue sections undergo dewaxing using organic solvents (such as xylene or toluene) and successive ethanol baths before histological staining or labelling. Consequently, several studies have focused on the so-called dewaxing protocol and its impact on recording Raman spectra [31, 32]. It is worth mentioning that some applications also aimed to develop a numerical dewaxing method by subtracting the paraffin peaks from vibrational signatures [33, 34].

More specifically, in the context of human skin analysis, Ali et al. demonstrated, using Fourier Transformed Infrared spectroscopy (FTIR) and CRS, drastic alterations in the biochemical composition of samples, especially in lipid content, when comparing dewaxed samples to unprocessed samples [35].

The present study is the first investigation focusing on the effects of formalin fixation, the most prevalent fixative agent, on Reconstructed Human Epidermis (RHE) skin models. This is accomplished through the application of CRS coupled with Principal Component Analysis (PCA). PCA is chosen as a multivariate method to examine the variance in the spectral data sets, and in particular the differences induced as a result of formalin fixation. Due to technical, economical, and ethical limitations, *In Vitro* Permeation Test (IVPT) using Franz diffusion cells [36], has become the gold standard method referenced in international guidelines [37–40]. Most commonly, excised human skin collected from plastic surgery and stored at -20°C or lower for up to one year [41–43], is considered acceptable for all compounds that are not dermally metabolized (OECD recommendations) [37]. Although several studies have shown a higher penetration of API and ACI in Reconstructed Human Epidermis (RHE) models compared to excised human skin [44–47], they are increasingly recognized as relevant substitutes to human biopsies. In this study, RHE samples were fixed with 10% Neutral Buffered Formalin (NBF) for 24 hours and stored in a dark cold room (4°C) for various periods (up to 21 days) to investigate the skin barrier function at both molecular and functional levels. Firstly, CRS coupled with PCA was employed to identify spectral features modified by the formalin fixation protocol, exploring changes in biochemical composition and organization across different skin layers. Secondly, the results from IVPT using caffeine, a common model compound, were examined to correlate skin barrier integrity with observed Raman features.

2. Materials and methods

2.1 Chemicals

Caffeine was purchased from Sigma-Aldrich (St. Quentin Fallavier, France), ultrapure water Elix® from Merck (Darmstadt, Germany), and 10 % Neutral Buffered Formalin (NBF) from Leica (Nanterre, France). Methanol and Dulbecco's Phosphate Buffered Saline (D-PBS) were purchased from Fisher scientific (Illkirch, France).

2.2 Reconstructed Human Epidermis (RHE)

Reconstructed human epidermis (RHE) samples were purchased from EpiSkin® (Lyon, France). The RHE are epidermal cultures (large model, 1.07 cm^2 diffusional area) consisting of a stratified and totally differentiated epidermis derived from human keratinocytes deposited on a collagen matrix (type I and type IV). The RHEs are shipped in 12-well plates after 13 days of

maturation. Upon delivery, RHE were deployed following the supplier's instructions. The inserts were transferred under aseptic conditions and at room temperature to a new, sterile 12-well plate. Each well of the new plate was filled with 2 mL of fresh culture medium provided by the manufacturer. The RHE were then placed in an incubator (37 °C, 5% CO_2) overnight.

2.3 Samples preparation

The day after receiving the RHE samples, 9 out of the 12 inserts were removed from the incubator and then fully immersed in 10% NBF for fixation at room temperature for 24 hours. The formalin fixation protocol is a slow process taking 2 to 24 h, since the diffusion of formalin is approximately 1 mm of tissue thickness for each hour of fixation [48], as formaldehyde must dissociate from methylene glycol (the hydrated form of formalin) to form covalent bonds with the molecular components of the sample [26]. All Fixed-RHE were placed in a dark cold room (4°C) until the day of the permeation experiment. The remaining 3 RHE samples (hereafter identified as 'FRESH') were kept in the incubator for 24h to synchronise all samples for the permeation experiments. At T0 (i.e. at the end of the 24h fixation protocol), T0+7 days and T0+21 days, permeation experiments were carried out, in triplicate, on FRESH T0, FIXED T0, FIXED T0+7 and FIXED T0+21. Un-fixed (FRESH) samples were used as control only for the T0 samples.

Additional RHE samples, reserved for CRS analysis, not exposed to caffeine, were prepared at T0 (FRESH, n=1 and FIXED T0, n=1), T0+7 days (FIXED T0+7, n=1) and at T0+21 days (FIXED T0+21, n=1). The samples were taken out of the cold room (4 °C) and placed at -20°C until analysis using CRS.

2.4 Confocal Raman Spectroscopy

Twenty micrometre thin sections were prepared from RHE samples which were not exposed to caffeine using a cryostat (Leica CM 1850 UV, Nanterre, France). Sections were placed onto histology glass slides for CRS analysis. Raman spectra was collected using an Alpha300R Raman microscope (WiTec, Ulm, Germany) equipped with 532 nm laser source. To avoid photodamaging, the power was set to 10 mW at the sample. A 600 lines/mm grating was selected, and the back scattered light was collected on a back illuminated deep depletion CCD detector over the spectral range 0-3600 cm^{-1} with a spectral resolution ~5 cm^{-1}. Given the inherent heterogeneity of the RHE models, it is important to note that spectral variations can occur due to differences in sampling positions and sample conditions. To mitigate these

effects, the data were recorded using a 50X objective with a numerical aperture of 0.5 (Olympus, NA=0.5), resulting in an increased spot size of approximately 1.3 µm. This approach helps to average out local variations and provides a more representative spectral profile. The acquisition time was set to 10 sec x 2 accumulations. The instrument is calibrated daily using a 2-step procedure. Firstly, the True Cal function of Project 5 (WITec, Ulm, Germany) is used. It is an automatic multipoint calibration routine performed with a Mercury-Argon (HgAr) light source integrated in the Raman microscope. Secondly, prior to data acquisition, a verification was done using the peak at 520.7 cm^{-1} from a silicon substrate. The layers of the RHE skin model can be observed from the bright field image (**Figure 1)** enabling to target a specific area to collect the Raman spectra. A total of 2300 spectra were acquired per sample, distributed between the SC (800 spectra), the viable epidermis (600 spectra) and the support membrane (900 spectra).

2.5 Raman data analysis

Data analysis was performed using Matlab® (MathWorks, USA). A Lieber baseline correction was applied [49], using a linear correction function with 10 iterations, followed by a unit vector normalisation. The fingerprint region (FPR) between (800 - 1800 cm^{-1}) and the high wavenumber region (HWR) (2500 - 3700 cm^{-1}) were analysed.

Multivariate analysis: Principal Components Analysis (PCA) is an unsupervised multivariate analysis technique used to evaluate the variability and to simplify a complex data set of multiple dimensions. It allows the reduction of the number of variables in a multidimensional data set, although it retains most of the variation within the data set. The other advantage of this method is the derivation of PC loadings which represent the variance of each variable (wavenumber) for a given PC, hence reflecting the variations in the chemical components contributing to the spectra [18]. In the scatter plot, the first principal component (PC1) accounts for the highest explained variance. Moreover, each dot in the scatterplot, corresponding to a spectrum, can be located in space using the coordinates defined by the scores along both PC1 and PC2. Therefore, similar spectra tend to be gathered with relatively close PC scores while the presence of significant variations in spectral features will result in higher distances between spectra.

2.6 Caffeine permeation assay

Permeation experiments were performed with RHE samples directly in their culture inserts placed in the 12-well plates, as previously reported by Dancik et al., [50]. FRESH T0, FIXED T0, FIXED T0+7 or FIXED T0+21 samples were transferred in 12 well plates and equilibrated for 30 min at 37 °C. 2 mL of D-PBS was used as the receptor medium. A 2% w/w (20mg/mL) PBS served as the donor solution. A volume of 200 µL was applied directly onto each RHE sample. The time-dependent permeation of caffeine was followed over 12 hours. At specific time intervals (every 30 min from 0.5 to 2.5 h then every 60 min from 3 h until 12h), the 2 mL of receptor medium was collected for analysis by High Performance Liquid Chromatography (HPLC). Following the collection of the receptor fluid, each RHE was immediately transferred to a new well, and filled with 2 mL of fresh D-PBS [50].

At the end of the permeation experiment, additional steps were performed for determining mass balances. The donor solutions were removed and set aside for analysis by HPLC. RHE and support membranes were then carefully removed from the inserts using a punch and separated. The SC side of the RHE and receptor side of the support membrane were gently swabbed with cotton tips which were then immersed in 2 mL methanol for extraction and analysed by HPLC. The SC side of the tissue was washed for 30 s with methanol to remove any caffeine residue. Skin and support membranes were cut into small pieces and likewise immersed in 2 mL methanol for 12 hours and the extracted solution was then analysed by HPLC.

2.7 HPLC analysis

The receptor media, donor solutions, extracts from skin and support membranes were analysed by HPLC. The HPLC system (Ultimate 3000, Dionex) consisted of a UHPLC pump; an auto-injector; a diode array detector and an Interchim Kromasil Vintage Series C18 column (4.6 x 150 mm, 5 µm). The detection wavelength for caffeine was 272 nm. The temperatures of the column and the auto-injector were set to 25 °C and 15 °C, respectively. The mobile phase used in isocratic mode was methanol 50%: water 50% (v/v) + 10 mM of phosphoric acid. The injection volume of samples was 10 µL. The duration of the analysis of each sample was 6 min at a flow rate of 1 $ml.min^{-1}$. The software used was Chromeleon 7.1 (Thermo Scientific).

A standard calibration curve was prepared prior to analysis. Standards were obtained in triplicate by dissolving caffeine in PBS at concentrations of 1, 5, 10, 100 and 500 $\mu g\ min^{-1}$. The observed retention time was 2.620 ± 0.008 min.

2.8 HPLC Data analysis

Results are presented as a plot of the cumulative mass of permeated caffeine per area of skin model (mg cm^{-2}):

$$Q_{\mathrm{n}} = \frac{C_{\mathrm{n}} \times V_{\mathrm{rec}} + \sum_{i=1}^{i=n-1} C_{\mathrm{i}} \times V_{\mathrm{i}}}{S} \quad \textbf{(1)}$$

Q_n (mg cm^{-2}) is the cumulative mass of caffeine at a time *n*, normalised by the diffusion surface S, C_n (mg cm^{-3}) is the concentration of the receptor medium determined by HPLC, V_{rec} the volume of the receiving compartment volume of receptor medium = 2 mL), C_i the concentrations calculated at the previous time interval and V_i the sample volume (here V_i = V_{rec}).

Three additional parameters characterizing caffeine permeation were calculated to compare the results between formulations. The steady-state flux (J_{ss} = dQ/dt, expressed in µg cm^{-2} h^{-1}) is equal to the slope of the cumulative amount profile in the steady-state (linear) portion of the profile. The lag time (t_{lag}, expressed in h) is the delay required for diffusion through the skin to reach a steady-state. It is determined as the intercept of the Q(t) profile extrapolated to the time axis [51, 52]:

$$Q(t) = J_{\mathrm{SS}}\left(t - t_{\mathrm{lag}}\right) \quad \textbf{(2)}$$

The permeability coefficient (Kp, expressed in cm h^{-1}) represents the "speed" of penetration of the active ingredient and is obtained from:

$$K_{\mathrm{p}} = J_{\mathrm{SS}} / C_{\mathrm{d}} \quad \textbf{(3)}$$

where C_d is the applied donor concentration in µg cm^{-3}.

All results are reported as mean ± SD (n=3). The statistical significance of the data was determined using the Student's t-test with a level of significance set for p-values ≤ 0.05.

3. Results

3.1 Characterisation of the effects of fixation on RHE models by CRS

The RHE models are a stratified and fully differentiated epidermis [50], which is histologically comparable to human skin. The three main layers observed are the *stratum*

corneum (SC), the viable epidermis (VE), and the polymeric support membrane (PSM) composed of polycarbonate, according to supplier's description (**Figure 1**) [50, 53]. Despite the potential for biological variability, the rigorous standardization procedures and quality control measures employed with EpiSkin® RHE models ensure consistent layer depth and shape. This consistency is corroborated by previous investigations by Kichou et al. (2023) and Dancik et al. (2020) [14, 50], as well as the uniformity observed in cryomicrotome sections illustrated in Figure 1.

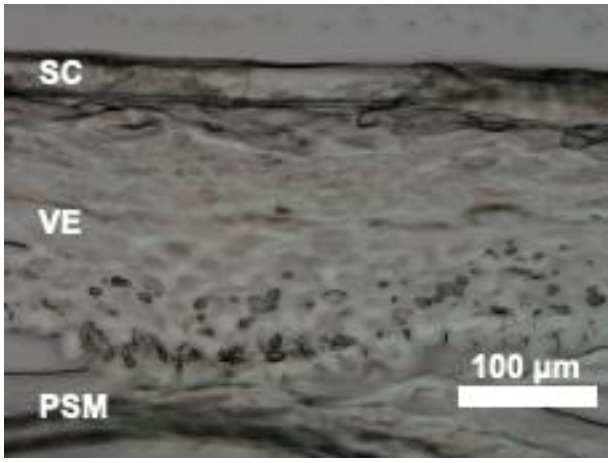

Figure 1: *Representative bright field image of FRESH RHE thin section taken with an x40 objective. Stratum corneum (SC), viable Epidermis (VE) and polymeric support membrane (PSM).*

3.1a *Stratum corneum*

Mean spectra for the fingerprint region (FPR) and the high wavenumbers region (HWR) are presented in supplementary materials (**Figure S1**). The main features corresponding to proteins and lipids can be observed and the corresponding assignments can be found in the literature [53, 54]. For the purpose of this study, PCA was used to highlight the spectral difference between FRESH and FIXED samples.

The PCA scatter plot for the FPR is presented in **Figure 2a**, the distribution of the data illustrating the heterogeneity of the samples at a microscopic level. Along PC1, which accounts for 53.7% of the explained variance, there was no clear discrimination observed between FRESH T0 (red dots), FIXED T0 (green dots), FIXED T+7 (blue dots), and FIXED T+21 (black dots). However, along PC2, which accounts for 13.5% of the explained variance, the

discrimination between FRESH (red dots) and FIXED samples was more pronounced, with reduced overlapping of dots. It is worth noting that no contribution from the formalin was observed in principal components (**Figure S4**). The loading of PC1 (**Figure 2b**) had the most intense features at 1655 cm^{-1} (negative band -N–C=O deformation, Amide I band), 1440 and 1469 cm^{-1} (C–H scissoring from proteins and lipids), 1380 cm^{-1} (CH_3 bending or deformation of lipid), 1302 cm^{-1} (C–H deformation of Amide III), 1127 cm^{-1} (trans-conformation of lipid), 1060 cm^{-1} (C-C skeletal stretching of lipid), 1027 cm^{-1} (C-H bending or deformation of phenylalanine), 1005 cm^{-1} (negative band -C–C=C deformation, aromatic acids from phenylalanine), 958 cm^{-1} (negative band -CH_2 deformation for cholesterol) and 854 cm^{-1} (fermi doublet ring for tyrosine). There was no clear correlation between the features observed and the effects of formalin fixation. However, the FIXED samples show a greater variance according to PC1, stretching toward positive scores, although there is no discernible difference between the samples stored for different times. The corresponding positive features observed in the loading 1 highlighted a higher heterogeneity in lipids distribution, notably ceramides [55]. The loading of PC2 (**Figure 2b**) exhibits main features at 1670 cm^{-1} (negative band- C=O deformation coupled to a N-H deformation, Amide I band), 1655 cm^{-1} (N–C=O deformation, Amide I band), 1585 cm^{-1} (C-C bending or deformation of phenylalanine, 1555 cm^{-1} (C=C stretching for tryptophan), 1440 - 1469 cm^{-1} (C–H scissoring from proteins and lipids), 1380 cm^{-1} (CH_3 bending or deformation of lipid), 1339 cm^{-1} (negative band - C-C stretching and C-H bending of phenylalanine and tryptophan), 1302 cm^{-1} (C–H deformation of Amide III), 1157 cm^{-1} (C-C stretching, CH_3 rocking and C-C skeletal conformation of ceramides), 1127 cm^{-1} and 1064 cm^{-1} (trans-conformation and skeletal trans-conformation of lipid), 1027 cm^{-1} (C-H bending or deformation of phenylalanine), 1005 cm^{-1} (negative band - C–C=C deformation, aromatic acids from phenylalanine), 987 cm^{-1} (C-C stretching β-sheet conformations proteins) and 854 cm^{-1} (Fermi doublet ring for tyrosine). These variations can be more specifically assigned to the fixation protocol. Formalin is known to trigger intermolecular bridges of the aldehyde groups with reactive groups in cells and tissue by cross-linking of proteins (tyrosine rings) [7]. However, it was observed that the modifications extended from significant modifications in the Amide I random chain and β-sheet conformations, alterations in phenylalanine residues, tryptophan, and the Fermi doublet ring of tyrosine to structural changes in the lipid region, particularly in the skeletal conformation and skeletal trans-conformation of lipids. The scatter plot for the HWR (**Figure 2c**) showed no discrimination of the data along PC1 or PC2, accounting for 92% and 2.8% of explained variance, respectively. The distribution of the data reflects most likely the biochemical heterogeneity of the SC without correlation with

effects from the formalin fixation protocol. The most intense features in loading 1 and loading 2 (**Figure 2d**) are at 2854 cm^{-1} and 2885 cm^{-1} (negative bands - CH_2 asymmetric stretching of lipids and proteins, mostly ceramides), 2930 cm^{-1} (CH_3 symmetric stretching of ceramides), 2970 cm^{-1} (CH_3 symmetric stretching of ceramides), 3063 cm^{-1} (=CH stretching of ceramides) and a broad band from 3200 - 3700 cm^{-1} (O–H) suggested variations in lipid and protein contents across samples [55, 56].

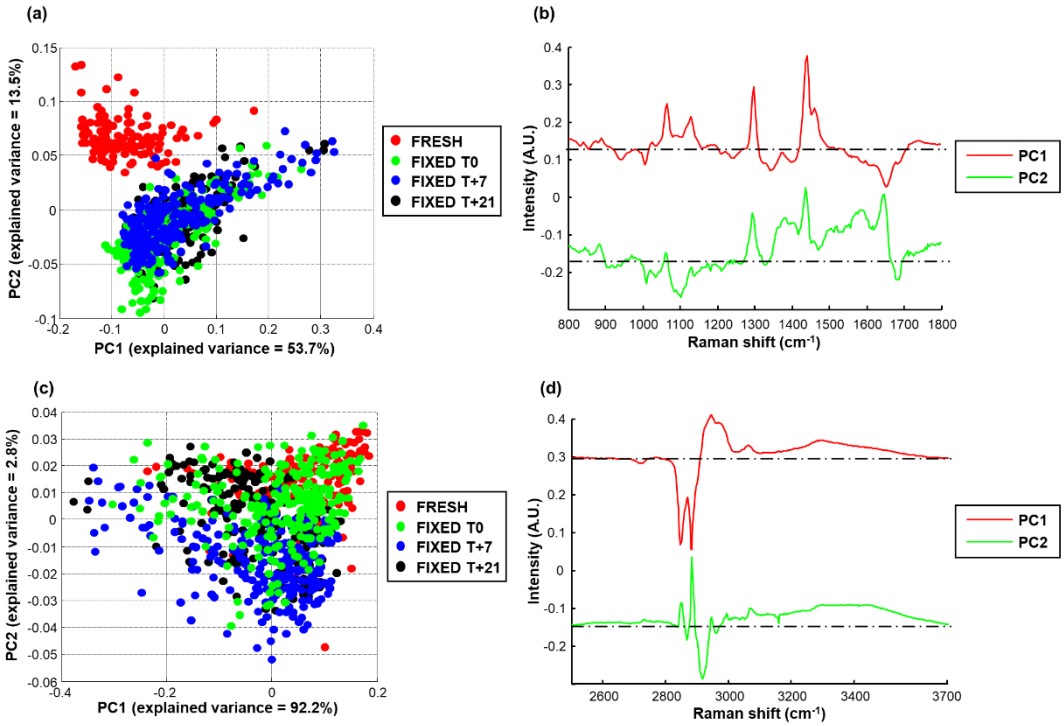

Figure 2: *PCA for spectra collected on the stratum corneum layer: (a) Scatter plot for PC1 and PC2 in the fingerprint region (800 – 1800 cm^{-1}) and (b) the corresponding loadings. (c) Scatter plot for PC1 and PC2 in the high wavenumbers region (2500 -3700 cm^{-1}) and (d) the corresponding loadings. Spectra are offset for clarity.*

3.1.b Viable epidermis

The mean Raman spectra recorded from the VE are provided in supplementary materials (**Figure S2**). The PCA scatter plots are presented in **Figure 3**. For the FPR (**Figure 3a**), a clear discrimination was observed between FRESH T0 (red dots) and FIXED T0 (green dots), FIXED

T+7 (blue dots) and FIXED T+21 (black dots) along PC1 (25.5% of the explained variance). However, there is no discrimination along PC2 (17.3 % of the explained variance).

The loading of PC1 (**Figure 3b**) displays features at 1726 cm^{-1} (C=O) stretching for amino acids), 1698 cm^{-1} (C=O coupled to a N-H deformation of Amide I band), 1655 cm^{-1} (negative band - N–C=O deformation, Amide I), 1608 cm^{-1} (C=C deformation in plane mode of phenylalanine and tyrosine), 1576 cm^{-1} (C=C deformation mode of phenylalanine), 1555 cm^{-1} (C=C stretching for tryptophan), 1440 and 1469 cm^{-1} (C–H scissoring from proteins and lipids), 1302 cm^{-1} (C–H deformation of Amide III), 1284 cm^{-1} (C-H deformation for α helix of Amide III), 1252 cm^{-1} (random coil of Amide III (secondary structure), 1207 cm^{-1} (C-C6-H5 stretching for phenylalanine, tryptophan, and tyrosine), 1178 cm^{-1} (C-H for phenylalanine and tyrosine), 1138 cm^{-1} (C-N, C-C stretching of skeletal trans conformation of lipid), 1102 cm^{-1} (gauche conformation of lipid), 1060 cm^{-1} (C-C skeletal stretching of lipid), 1027 cm^{-1} (C-H bending or deformation of phenylalanine), 1005 cm^{-1} (negative band - C–C=C deformation, aromatic acids from phenylalanine), 987 cm^{-1} (C-C stretching β-sheet conformations proteins), 923 cm^{-1} (C-C stretching of a-helix for proteins), 902 cm^{-1} (C–O–C skeletal mode of lipid), 854 and 824 cm^{-1} (Fermi doublet ring for tyrosine) [54, 55]. The VE displayed numerous effects from the fixation protocols across the entire FPR region and, similarly to the SC, both proteins and lipids are affected. These observations are consistent with some degree of molecular reorganisation induced by formalin within the deeper layers of skin.

The loading 2 (**Figure 3b**) displayed features at 1683 cm^{-1} (C=O coupled to a N-H deformation of Amide I band), 1655 cm^{-1} (negative band - N–C=O deformation, Amide I), 1440 and 1469 cm^{-1} (C–H scissoring from proteins and lipids), 1302 cm^{-1} (C–H deformation of Amide III), 1284 cm^{-1} (C-H deformation for a helix of Amide III), 1252 cm^{-1} (random coil of Amide III (secondary structure), 1198 cm^{-1} (C-C6-H5 stretching for phenylalanine, tryptophan, and tyrosine), 1178 cm^{-1} (C-H for phenylalanine and tyrosine), 1127 cm^{-1} (C-N, C-C stretching of skeletal trans conformation of lipid), 1102 cm^{-1} (gauche conformation of lipid), 1060 cm^{-1} (C-C skeletal stretching of lipid), 1027 cm^{-1} (C-H bending or deformation of phenylalanine), 1005 cm^{-1} (negative band - C–C=C deformation, aromatic acids from phenylalanine), 987 cm^{-1} (C-C stretching β-sheet conformations proteins), 923 cm^{-1} (C-C stretching of a-helix for proteins), 902 cm^{-1} (C–O–C skeletal mode of lipid) and 854 cm^{-1} (fermi doublet ring for tyrosine) [54, 55]. While these variations correspond to intra samples variability it is interesting to notice that the distribution of data is significantly larger for FIXED

samples than FRESH samples, suggesting that the fixation somehow increased the biological heterogeneity within FIXED samples.

The scatter plot for the HWR (**Figure 3c**) indicates a discrimination along PC1 and PC2, accounting for 74.7 % and 16.5% of explained variance, respectively. The data are organised into two diagonal clusters (FRESH (red dots) and FIXED T0 (green dots), FIXED T+7 (blue dots) and FIXED T+21 (black dots). Loading 1 and 2 (Figure 3d) showed similar features at 2854 cm^{-1} and 2885 cm^{-1} (negative bands - CH_2 asymmetric stretching of lipids and proteins, mostly Keratin), 2930 cm^{-1} (CH_3 symmetric stretching of keratin), 2970 cm^{-1} (CH_3 symmetric stretching of keratin), 3063 cm^{-1} (=CH stretching of keratin) and the large band from 3200 - 3700 cm^{-1} (O–H vibration). The results are consistent with variations in lipid and protein contents [57, 58].

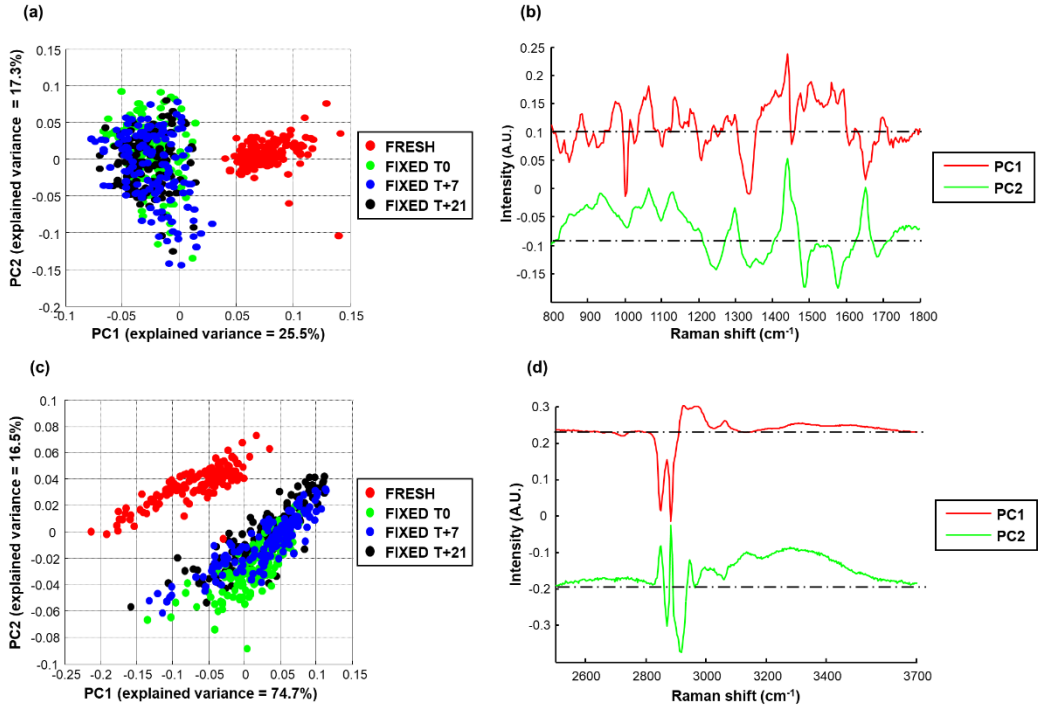

Figure 3: *Principal components analysis on the viable epidermis layer: (a) Scatter plot of the two first component on the fingerprint region (800 – 1800 cm^{-1}) and (b) the corresponding loadings. (c) Scatter plot of the two first component on the high wavenumbers region (2500 - 3700 cm^{-1}) and (d) the corresponding loadings. Spectra are offset for clarity.*

3.1.c Polymeric support membrane (PSM)

The mean spectra of PSM for the FPR and HWR are presented in supplementary materials (**Figure S3**). According to the manufacturer, the support membrane is composed of polycarbonate. However, such materials are known to be characterised by sharp and intense Raman features [59]. The maxima of the amide I band at 1655 cm^{-1} (N–C=O deformation) with a pronounced shoulder at 1671 cm^{-1}, the double feature at 1269 cm^{-1} (C-H deformation for α helix of Amide III) and 1244 cm^{-1} (random coil of Amide III (secondary structure), and the spectral pattern in the region 800 - 1000 cm^{-1} that displayed 2 peaks at 854 cm^{-1} and 936 cm^{-1} with 2 shoulders at 876 cm^{-1} and 920 cm^{-1} (amino acid side chain vibrations of proline and hydroxyproline and C-C stretching vibration) are evidences that collagen is found in the PSM composition [57, 58, 60].

The PCA scatter plot for the FPR is displayed in **Figure 4a**. No clear discrimination was observed between the FRESH samples (red dots), FIXED T0 (green dots), FIXED T0+7 (blue dots), and FIXED T0+21 (black dots) according to either PC1 or PC2, accounting for 24.3% and 14.7% of the explained variance, respectively. As observed for the other two over layers, the FRESH samples are fairly tightly grouped, while there is greater variance in the FIXED samples. It was observed that for PC1, the most spectra corresponding to FRESH T0 mainly had negative scores but the overlap with FIXED T0+21 prevent from assigning specific variations due to fixation. Loading 1 and 2 (**figure 4b**) exhibit features at 1726 cm^{-1} (C=O) stretching for amino acids), 1698 cm^{-1} (C=O coupled to a N-H deformation of Amide I band), 1655 cm^{-1} (N–C=O deformation, Amide I), 1608 cm^{-1} (C=C deformation in plane mode of phenylalanine and tyrosine), 1576 cm^{-1} (C=C deformation mode of phenylalanine), 1555 cm^{-1} (C=C stretching for tryptophan), 1440 and 1469 cm^{-1} (C–H scissoring from proteins), 1302 cm^{-1} (C–H deformation of Amide III), 1284 cm^{-1} (C-H deformation for α helix of Amide III), 1252 cm^{-1} (random coil of Amide III (secondary structure), 1207 cm^{-1} (C-C6-H5 stretching for Hydroxyproline and Tyrosine), 1178 cm^{-1} (C-H for phenylalanine and tyrosine), 1138 cm^{-1} (C-N, C-C stretching of protein), 1027 cm^{-1} (C-H bending or deformation of phenylalanine), 1005 cm^{-1} (negative band - C–C=C deformation, aromatic acids from phenylalanine), 987 cm^{-1} (C-C stretching β-sheet conformations proteins), 923 cm^{-1} and 854 cm^{-1} (amino acid side chain vibrations of proline and hydroxyproline and C-C stretching vibration of the collagen backbone) [58, 60]. The scatter plot representing the HWR (**Figure 4c**) did not exhibit any discrimination of the data along PC1 and PC2 axes, which accounted for 41 % and 20.6 % of the explained variance, respectively. The most intense features in loading 1 and loading 2 (**figure 4d**) are at

2868 cm^{-1} and 2885 cm^{-1} (CH_2 asymmetric stretching of protein), and 2940 cm^{-1} to 3063 cm^{-1} (CH stretching of protein) [57, 61].

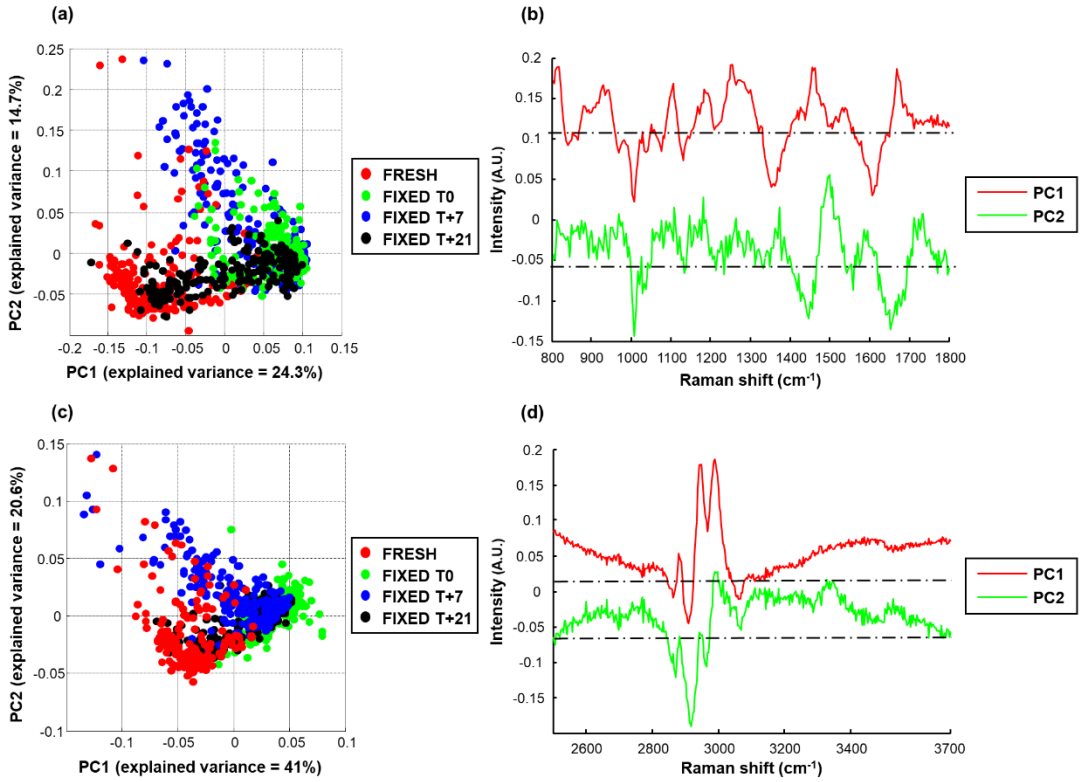

Figure 4: *Principal component analysis on the polymeric support membrane: (a) Scatter plot of the two first components on the fingerprint region (800 - 1800 cm^{-1}) and (b) the corresponding loadings. (c) Scatter plot of the two first components on the high wavenumbers region (2500 - 3700 cm^{-1}) and (d) the corresponding loadings. Spectra are offset for clarity.*

3.2 Determining the effect of formalin fixation on RHE models permeability to caffeine

Caffeine is a small, hydrophilic compound of the methylxanthine class [62], which has been employed in several cosmetic preparations and it is recognized as a reference substance for *in vitro* skin absorption tests using Franz diffusion cells by the OECD [63, 64]. **Figure 5** shows the 12-hour cumulative amount permeated through RHE for FRESH T0 (red), FIXED T0 (green), FIXED T0+7 (blue) and FIXED T0+21 (black) exposed to 2 wt% caffeine solutions.

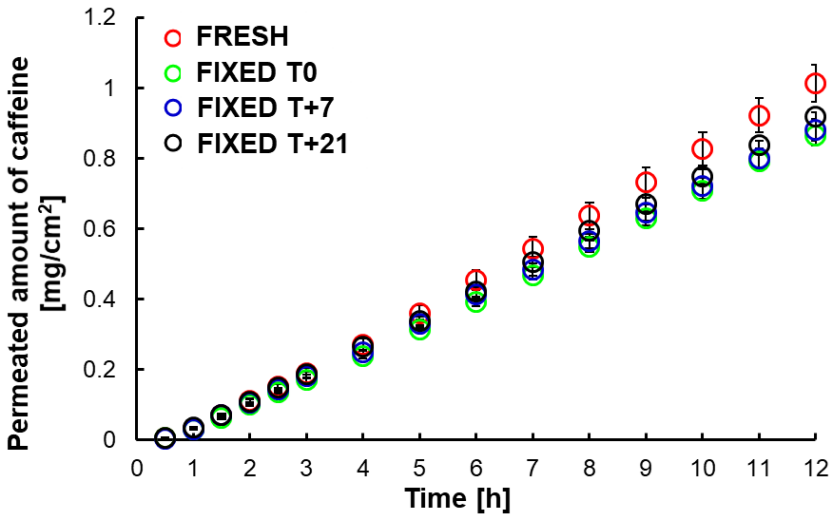

Figure 5*: Cumulative amount of caffeine permeated through RHE as function of time. (**red**: FRESH T0. **green**: FIXED T0. **blue**: Fixed T0+7. **black**: FIXED T0+21). Data shown as means ± SD (n =3).*

After 30 min, the cumulative amounts of permeated caffeine were found to be 7.31 ± 0.6 µg.cm^{-2} for FRESH T0, 6.1 ± 0.5 µg.cm^{-2} for FIXED T0, 4.9 ± 0.1 µg.cm^{-2} for FIXED T0+7 and 6.9 ± 1.1 µg.cm^{-2} for FIXED T0+21. Significant differences were found between FRESH and FIXED T0 ($p=0.04$) and FIXED T0+7 ($p=0.02$). However, no significant difference was found between the FRESH T0 and FIXED T0+21 ($p= 0.58$). From 30 min to 8 hours, the cumulative amounts of caffeine similarly increased for all conditions studied with no statistical difference observed between FRESH T0 compared to FIXED T0 ($0.05 < p < 0.21$), FIXED T0+7 ($0.08 < p < 0.86$) and FIXED T0+21 ($0.13< p < 0.73$).

From 8 to 12 hours, FRESH T0 was found significantly different compared to FIXED T0, FIXED T0+7 and FIXED T0+21 ($0.02 < p < 0.04$). Ultimately, cumulative amounts at 12 hours were 1.01 ± 0.05 mg.cm^{-2} for FRESH T0, 0.86 ± 0.03 mg.cm^{-2} for FIXED T0 (corresponding to a decrease of 14%), 0.88 ± 0.03 mg.cm^{-2} for FIXED T0+7 (corresponding to a decrease of 13%) and 0.92 ± 0.01 mg.cm^{-2} for FIXED T0+21 (corresponding to a decrease of 9%).

Table 1 presents the different parameters calculated from the permeation curve. The steady state flux Jss ranged from 79 ± 3 µg.cm^{-2}.h^{-1} (Fixed T+7) to 94 ± 4 µg.cm^{-2}.h^{-1} (FRESH T0). Significant differences were found between FRESH T0 and all FIXED samples ($p<0.05$). No significant difference was, however, found between Fixed T0, Fixed T0+7 and Fixed T0+21 ($0.20 < p < 0.80$) (**Table 1**). The lag time to steady-state (t lag) was found to be 1.22 ± 0.17 h

for FRESH T0, 1.11 ± 0.06 h for FIXED T0 (10% shorter), 0.83 ± 0.01 h for FIXED T+7 (32% shorter) and 0.88 ± 0.17 h for FIXED T+21 (28% shorter). No significant differences were found between FRESH T0 and FIXED T+21 ($0.1 < p < 0.22$), although significant differences were observed compared to FXED T+7 ($p = 0.02 < 0.05$). The permeability coefficient (K_p) for FRESH was 4.71 ± 0.18 $cm.h^{-1}$, 3.99 ± 0.15 $cm.h^{-1}$ for FIXED T0 (-15%), 3.95 ± 0.13 $cm.h^{-1}$ for FIXED T+7 (-16%) and 4.10 ± 0.04 $cm.h^{-1}$ for FIXED T+21 (-13%). Significant differences were found between FRESN T0 and fixed samples ($0.01 < p < 0.03$). However, no significant differences were found between FIXED T0, FIXED T+7 and FIXED T+21 ($0.20 < p < 0.80$).

Table 1: *Steady state fluxes (J_{ss}), lag times (t_{lag}), permeability coefficients (k_p) obtained from cumulative amount profiles of caffeine through RHE samples (FRESH, FIXED T0, FIXED T+7and FIXED T+21). All data displayed as mean ± standard deviation of n = 3 experiments.*

	J_{SS} [µg .cm^{-2}.h^{-1}]	t_{lag} [h]	k_p [10^{-3}.cm .h^{-1}]
FRESH	*94.06 ± 3.69*	*1.22 ± 0.17*	*4.71 ± 0.18*
FIXED T0	*79.63 ± 2.91*	*1.10 ± 0.06*	*3.99 ± 0.15*
FIXED T+7	*79.01 ± 2.69*	*0.83 ± 0.01*	*3.95 ± 0.13*
FIXED T+21	*81.83 ± 0.75*	*0.88 ± 0.17*	*4.10 ± 0.04*

4. Discussion

The effectiveness of a topical product is directly tied to the capability of its active ingredients to overcome the skin barrier [65]. Therefore, when testing new products or demonstrating the equivalence of generic products to the original [37], IVPT using Franz diffusion cells [36], has become the gold standard method referenced in international guidelines [37–40]. Due to limited access to human samples, the common practice is to store skin biopsies frozen. However, many studies in the literature have reported that exposing excised human skin to negative temperatures (-20°C, -85°C) for varying durations (ranging from 1 week to 1 year) leads to a significant increase in permeability due to the formation of small ice crystals [66], that disrupts the barrier function [67–73]. For instance, Nielsen et al. reported that the storage

of excised abdominal human skin biopsies at -80°C for 21 days increased, up to four-fold, the permeability coefficient of caffeine compared to fresh skin [70]. While a 1.6-fold increase in the cumulative amount of chromone acid permeating through excised human epidermis was observed after a short period of storage for 2.5 days at -17°C [68], prolonged storage for 10 days at -60°C and 3 weeks at -80°C resulted in a 2.4-fold higher flux of trichothecene mycotoxin in full-thickness human thigh skin [74], and a 4-fold increase of permeability coefficient for caffeine in excised abdominal skin [70], respectively. Pig skin has been extensively used as a model due to its close resemblance to human skin, particularly for studying the effects of freezing. For instance, Sintov et al. observed that storing pig skin at -20°C for 7 days led to a 2- to 8-fold increase in the permeability coefficient of caffeine [72]. Similarly, Abdayem et al. demonstrated that the permeability coefficient of caffeine in pig ear skin increased by up to 4 to 5 times after 1 day of storage at -20°C, compared to fresh skin [73]. For substances like Diclofenac sodium and L-DOPA (3,4-dihydroxyphenylalanine), permeation fluxes were found to be 5-fold and 3.8-fold higher, respectively, in frozen pig ears stored at -20°C for two weeks [75]. Additionally, acyclovir and methyl salicylate showed an 8-fold and 2-fold increase in cumulative permeated amounts in porcine ear skin when stored at -20°C for 6 weeks [76]. All the experiments conducted on human skin and pig skin resulted in a common pattern of increasing permeability following the freezing of the samples. Despite variabilities related to the molecule tested and experimental design (temperature, duration of storage, etc.), the studies consistently reported a substantial increase in cumulative amounts, representing a multiple-fold increase compared to fresh skin. In contrast, the cumulative amount for caffeine permeating through the RHE model presently studied tends to decrease in samples that have been fixed **(Figure 5)**, suggesting that the effects of chemical fixation differ from the physical disruption of the skin barrier caused by freezing. Also, it is worth noting that after 12 hours, the quantity of caffeine that permeated through the FIXED RHE models was comparable to that of FRESH samples, with, at most, a 15% reduction (0.85-fold lower), which is significantly less than any reported data for freezing protocols. The data on accumulated caffeine amounts and the calculated permeation parameters indicated that the barrier in FIXED samples remained functional, albeit with reduced permeability. Similarly, steady-state fluxes and permeability coefficients indicated lower caffeine permeability. The 24-hour fixation protocol did not cause damage to the RHE models, and the limiting diffusion rate was preserved.

Although less studied for RHE, the impairment of the skin barrier function due to freezing has been reported by Dancik et al. in the case of resorcinol (a small hydrophilic compound)

[50]. Storage of RHE at -150°C, -80°C, and -20°C for 1 and 10 weeks resulted in an increased permeability ranging from 3 to 6-fold compared to fresh samples. RHE models are matured, fully stratified 3D models which mimic the physical and chemical barrier of human skin [77], and as such their behaviour to freezing is consistent with the effects of impairment of the barrier function observed in human skin using a small hydrophilic compound such as caffeine [70]. Although a direct comparison between caffeine and resorcinol may pose challenges, it is apparent that consistently storing samples below freezing substantially increase the permeability of skin samples while, in comparison, the present result highlights that chemical fixation with formalin leads to minimal modification (i.e. decrease). Formalin is a well-established fixative, used in histology to preserve the structural and morphological characteristic of biological tissues [8, 29, 78]. However, it use on skin samples before conducting permeation studies need to be further been investigated. For instance, the used cryoprotective agents, such as 10% glycerol, as preventive method to limit the damage to the skin during freezing [66, 79, 80] can induced cytotoxicity, dehydration and modification of the lipid structure may resulting in compromised integrity of the *stratum corneum* and a reduced barrier function [79, 81–83]. Therefore, the present study described a relevant alternative using formalin to chemically fix the samples.

With regards to the observations made by CRS, it is well-known that formalin forms covalent bonds with the biochemical components of the sample, resulting in compositional and conformational changes, particularly in proteins and lipids [84]. The examination of both FRESH and FIXED samples revealed notable alterations in proteins, specifically in the Amide I random chain, β-sheet conformation, α-helix, and random coil secondary structures in Amide III. Additionally, there were observable changes in phenylalanine residues, tryptophan, and the Fermi doublet ring of tyrosine. Notably, modifications in lipids were also identified, including shifts in the skeletal trans-conformation and gauche conformation of lipids. These changes were particularly pronounced in the viable epidermis, which has a higher protein content compared to the *stratum corneum* and the polymeric support membrane layers. The formalin-induced effects observed in this study are consistent with other studies, demonstrating the usefulness of the fixation process for single cell analysis by spectroscopic methods, and also the alterations it induces in the protein and lipid components [28, 84, 85]. Meade et al. have reported that the fixation in formalin alters the vibrational freedom of membrane lipids by modifying the lipid CH scissoring and C-C skeletal conformational modes, possibly through a reaction of methylene glycol in aqueous formalin with unsaturated hydrocarbon chains [84]. Ó Faoláin et al. have reported that the formalin fixation process leads to shifts in the Amide bands that are

attributed to alterations in protein conformation and potential cross-linking. These changes are caused by the methylene glycol component of aqueous formalin [85]. Draux et al. have shown that formalin fixation of cancer cells can induce several changes in spectral information assigned to proteins, notably a shift in the Amide region (Amide I and Amide III) due to changes in protein conformation [28]. Clearly, formalin fixation induces molecular modifications that can be witnessed in Raman spectral signatures a single cell level. However, at the functional level of the skin barrier the permeation assay demonstrated limited impact from the biochemical re-organisation resulting from the fixation protocol.

Bakar et al., using chromatography coupled with mass spectrometry, established that the functional barrier function in RHE was associated with the ceramide content in the SC. Furthermore, CRS revealed that the conformational order (Sskeleton) and the lateral packing (Sslat) of lipids, as indicated by the ratio of asymmetric deformation CH_2 (2880 cm^{-1}) / symmetric deformation CH_2 (2850 cm^{-1}), serves as an marker of the barrier function [86].

As described by Tfayli et al. [87], Sskeleton is calculated by dividing the intensity at 1080 cm^{-1} (indicating disordered packing towards a Hexagonal state) by the sum of intensities at 1130 cm^{-1} and 1060 cm^{-1} (reflecting ordered packing, towards an orthorhombic state). Presently, Sskeleton was found to be 0.45 for fresh RHE compared to 0.44 for FIXED T0, 0.44 for FIXED T+7, and 0.45 for FIXED T+21. The values highlighted no difference between fresh and fixed samples that exhibited low values indicating a ordered Inter Cellular Lipid (ICL) state in the SC [14, 88, 89]. The parameter Slat, calculated by dividing the intensities at 2880 cm^{-1} and 2850 cm^{-1} [87], also provides on the ICL packing state [14, 88, 89]. The Sslat values displayed of 1.90 for fresh RHE 1.87 for FIXED T0, 1.77 for FIXED T+7, and 1.79 for FIXED T+21 suggest low variations caused by fixation. Overall, these spectral markers for the conformational order and the lateral packing of lipids indicate a consistent lipid organisation between FRESH and FIXED RHE samples that support the preserved rate limiting skin barrier function observed trough IVPT after the fixation protocol. These observations by CRS are consistent with the formalin fixative having an effect on the proteins of the skin, while the integrity of the barrier function is known to be predominantly related to the specific lipid architecture in the *stratum corneum* [51]. It is noted that the structure and morphology of the RHE model, and changes to it at a microscopic level, have not been explored in any great detail, but could in the future be examined with the chemical sensitivity of confocal Raman imaging.

With regard to storing skin samples with formalin fixation, it is important to note that commercially available Reconstructed Human Epidermis (RHE) models typically come as

ready-to-use inserts that must be used within 48 hours of delivery, as per the manufacturer's recommendations. Many of these models are not available for individual purchase; instead, RHE samples are often conditioned in 12-well plates and sold by the dozen. Handling permeation studies involving multiple formulas with replicates can quickly become a labour-intensive task, particularly for laboratories lacking automated systems. Additionally, research has shown that the maturation of RHE models continues after delivery, leading to variations in the permeation of specific compounds over time [15]. Thus, the ability to store and maintain RHE models from a single batch (to mitigate inter-batch variability) at a consistent maturation stage holds significant relevance. Moreover, the standard 2-to-4-week delivery delay necessitates meticulous scheduling of experiments. Preserving sample integrity for a more flexible and cost-effective timeline would be a substantial asset to the field of dermal research. The present study has demonstrated that formalin fixation can maintain a stable barrier function over a storage period of 3 weeks, paving the way for more extensive permeation studies involving comparisons of multiple active ingredients and/or formulations that cannot be feasibly conducted within a single day.

Overall, this work has demonstrated that, despite spectral variability in the major biochemical components observed using CRS, the formalin fixation protocol does not impair the skin barrier function of the RHE samples. While freezing has been reported to greatly increase the permeability of caffeine, the permeation experiments have demonstrated a reduced penetration after fixation. Although additional investigation with model molecules having different physicochemical properties is necessary, the indications suggest that the fixation protocol could significantly reduce the workload and constraints of using RHE models simultaneously for permeation studies.

5. Conclusion

This work has demonstrated that the formalin fixation protocol offers a stable method for storing Reconstructed Human Epidermis (RHE) models without significantly compromising their barrier function. While molecular changes in various skin layers were observed by confocal Raman spectroscopy following the 24-hour fixation protocol, it is noteworthy that the permeation of caffeine remained consistent over a 3-week storage period. In comparison to documented effects of freezing in existing literature, formalin fixation resulted in only minor variations (approximately 10-15%) in the cumulative amount, time lag, flux, and permeability

coefficient for caffeine when compared to FRESH samples. Although further investigation is warranted to explore in more detail the specific changes of the biochemical structure of the RHE model, the study underscores that chemical fixation may be less detrimental than freezing, making it a promising alternative for storing skin samples that closely resemble native skin in terms of structure and morphology. Moreover, this study suggests that formalin fixation could effectively address one of the primary limitations associated with the use of RHE models in permeation studies: their limited shelf life.

Author Contributions: Conceptualization, F.B., H.J.B. and E.M.; methodology, H.K., F.B. and E.M. ; software, H.K. and F.B.; validation, F.B. and E.M.; formal analysis, H.K. and F.B.; investigation, H.K., A.C., and E.M.; resources, E.M. and I.C.; data curation, H.K. and F.B.; writing—original draft preparation, H.K., F.B., A.C., H.J.B., and E.M.; writing review and editing, H.K., A.C., F.B., H.J.B., and E.M.; visualization, H.K. and F.B.; supervision, F.B., and E.M.; project administration, F.B. and E.M.; funding acquisition, F.B. and E.M. All authors have read and agreed to the published version of the manuscript.

Funding: This research was funded by the Conseil Régional Centre-Val de Loire (Project ARD CVL MINIONs 2020-00141275 and UFO 2020-00138875). The Raman microspectrometer used is this study was funded by the FEDER (Fonds Europeen de Developpement Regional), grant number 2017-EX003256.

Conflict of interest: None to declare

References

1. Dancik Y, Jepps OG, Roberts MS (2007) 12 Beyond Stratum Corneum. Dermal Absorpt Toxic Assess 177:209

2. van Smeden J, Janssens M, Gooris GS, Bouwstra JA (2014) The important role of stratum corneum lipids for the cutaneous barrier function. Biochim Biophys Acta BBA - Mol Cell Biol Lipids 1841:295–313

3. Elias PM (1983) Epidermal Lipids, Barrier Function, and Desquamation. J Invest Dermatol 80:S44–S49

4. Barry BW, Edwards HGM, Williams AC (1992) Fourier transform Raman and infrared vibrational study of human skin: Assignment of spectral bands. J Raman Spectrosc 23:641–645

5. Williams AC, Edwards HGM, Barry BW (1992) Fourier transform Raman spectroscopy a novel application for examining human stratum corneum. Int J Pharm 81:R11–R14

6. Caspers PJ, Lucassen GW, Wolthuis R, Bruining HA, Puppels GJ (1998) In vitro and in vivo Raman spectroscopy of human skin. Biospectroscopy 4:S31–S39

7. Gazi E, Dwyer J, Lockyer NP, Miyan J, Gardner P, Hart C, Brown M, Clarke NW (2005) Fixation protocols for subcellular imaging by synchrotron-based Fourier transform infrared microspectroscopy. Biopolym Orig Res Biomol 77:18–30

8. Farhane Z, Bonnier F, Casey A, Maguire A, O'Neill L, Byrne HJ (2015) Cellular discrimination using in vitro Raman micro spectroscopy: the role of the nucleolus. Analyst 140:5908–5919

9. Byrne HJ, Bonnier F, Farhane Z (2019) Two-dimensional correlation analysis of Raman microspectroscopy of subcellular interactions of drugs in vitro. J Biophotonics 12:e201800328

10. Farhane Z, Bonnier F, Maher MA, Bryant J, Casey A, Byrne HJ (2017) Differentiating responses of lung cancer cell lines to Doxorubicin exposure: in vitro Raman micro spectroscopy, oxidative stress and bcl-2 protein expression. J Biophotonics 10:151–165

11. Huser T, Chan J (2015) Raman spectroscopy for physiological investigations of tissues and cells. Adv Drug Deliv Rev 89:57–70

12. Lieber CA, Majumder SK, Billheimer D, Ellis DL, Mahadevan-Jansen A (2008) Raman microspectroscopy for skin cancer detection in vitro. J Biomed Opt 13:024013-024013–9

13. Zhao J, Lui H, Kalia S, Zeng H (2015) Real-time Raman spectroscopy for automatic in vivo skin cancer detection: an independent validation. Anal Bioanal Chem 407:8373–8379

14. Kichou H, Bonnier F, Dancik Y, Bakar J, Michael-Jubeli R, Caritá AC, Perse X, Soucé M, Rapetti L, Tfayli A (2023) Strat-M® positioning for skin permeation studies: A comparative study including EpiSkin® RHE, and human skin. Int J Pharm 647:123488

15. Bakar J, Michael-Jubeli R, El Khoury R, Hamla S, Assi A, Baillet-Guffroy A, Tfayli A (2021) Assessment of the skin barrier function in the reconstructed human epidermis using a multimodal approach at molecular, tissue and functional levels. Analyst 146:4649–4658

16. Assi A, Tfaili S, Quatela A, Bonnier F, Baillet-Guffroy A, Tfayli A (2022) Studying the effects of suberythemal UV doses on the human stratum corneum by in vivo confocal Raman spectroscopy. Eur J Dermatol 32:338–346

17. Ali S, Bonnier F, Ptasinski K, Lambkin H, Flynn K, Lyng F, Byrne H (2013) Raman spectroscopic mapping for the analysis of solar radiation induced skin damage. Analyst 138:3946–3956

18. Miloudi L, Bonnier F, Tfayli A, Yvergnaux F, Byrne HJ, Chourpa I, Munnier E (2018) Confocal Raman spectroscopic imaging for in vitro monitoring of active ingredient penetration and distribution in reconstructed human epidermis model. J Biophotonics 11:e201700221

19. Stella A, Bonnier F, Tfayli A, Yvergnaux F, Byrne HJ, Chourpa I, Munnier E, Tauber C (2020) Raman mapping coupled to self-modelling MCR-ALS analysis to estimate active cosmetic ingredient penetration profile in skin. J Biophotonics 13:e202000136

20. Lunter D, Daniels R (2014) Confocal Raman microscopic investigation of the effectiveness of penetration enhancers for procaine delivery to the skin. J Biomed Opt 19:126015–126015

21. Crowther JM, Sieg A, Blenkiron P, Marcott C, Matts PJ, Kaczvinsky JR, Rawlings AV (2008) Measuring the effects of topical moisturizers on changes in stratum corneum thickness, water gradients and hydration in vivo. Br J Dermatol 159:567–577

22. Crowther JM, Matts PJ, Kaczvinsky JR (2012) Changes in stratum corneum thickness, water gradients and hydration by moisturizers. Treat Dry Skin Syndr Art Sci Moisturizers 545–560

23. Caspers PJ, Williams AC, Carter EA, Edwards HG, Barry BW, Bruining HA, Puppels GJ (2002) Monitoring the penetration enhancer dimethyl sulfoxide in human stratum corneum in vivo by confocal Raman spectroscopy. Pharm Res 19:1577–1580

24. Xiao C, Moore DJ, Rerek ME, Flach CR, Mendelsohn R (2005) Feasibility of tracking phospholipid permeation into skin using infrared and Raman microscopic imaging. J Invest Dermatol 124:622–632

25. Pudney PDA, Mélot M, Caspers PJ, van der Pol A, Puppels GJ (2007) An *In Vivo* Confocal Raman Study of the Delivery of Trans-Retinol to the Skin. Appl Spectrosc 61:804–811

26. Fox CH, Johnson FB, Whiting J, Roller PP (1985) Formaldehyde fixation. J Histochem Cytochem 33:845–853

27. Bonnier F, Knief P, Lim B, Meade AD, Dorney J, Bhattacharya K, Lyng FM, Byrne HJ (2010) Imaging live cells grown on a three dimensional collagen matrix using Raman microspectroscopy. Analyst 135:3169–3177

28. Draux F, Gobinet C, Sulé-Suso J, Trussardi A, Manfait M, Jeannesson P, Sockalingum GD (2010) Raman spectral imaging of single cancer cells: probing the impact of sample fixation methods. Anal Bioanal Chem 397:2727–2737

29. Dorney J, Bonnier F, Garcia A, Casey A, Chambers G, Byrne HJ (2012) Identifying and localizing intracellular nanoparticles using Raman spectroscopy. Analyst 137:1111–1119

30. Hobro AJ, Smith NI (2017) An evaluation of fixation methods: Spatial and compositional cellular changes observed by Raman imaging. Vib Spectrosc 91:31–45

31. Faoláin EÓ, Hunter MB, Byrne JM, Kelehan P, Lambkin HA, Byrne HJ, Lyng FM (2005) Raman spectroscopic evaluation of efficacy of current paraffin wax section dewaxing agents. J Histochem Cytochem 53:121–129

32. Fullwood LM, Griffiths D, Ashton K, Dawson T, Lea RW, Davis C, Bonnier F, Byrne HJ, Baker MJ (2014) Effect of substrate choice and tissue type on tissue preparation for spectral histopathology by Raman microspectroscopy. Analyst 139:446–454

33. Tfayli A, Gobinet C, Vrabie V, Huez R, Manfait M, Piot O (2009) Digital dewaxing of Raman signals: discrimination between nevi and melanoma spectra obtained from paraffin-embedded skin biopsies. Appl Spectrosc 63:564–570

34. Ibrahim O, Maguire A, Meade AD, Flint S, Toner M, Byrne HJ, Lyng FM (2017) Improved protocols for pre-processing Raman spectra of formalin fixed paraffin preserved tissue sections. Anal Methods 9:4709–4717

35. Ali SM, Bonnier F, Tfayli A, Lambkin H, Flynn K, McDonagh V, Healy C, Clive Lee T, Lyng FM, Byrne HJ (2013) Raman spectroscopic analysis of human skin tissue sections ex-vivo: evaluation of the effects of tissue processing and dewaxing. J Biomed Opt 18:061202–061202

36. Franz TJ (1975) Percutaneous Absorption. On the Relevance of in Vitro Data. J Invest Dermatol 64:190–195

37. No OT (2004) 428: skin absorption: in vitro method. OECD Guidel Test Chem Sect 4:1–8

38. European Commission. Directorate-General for Health and Consumers (2010) Basic criteria for the in vitro assessment of dermal absorption of cosmetic ingredients. European Commission, BE

39. FDA U (2018) Bioanalytical method validation guidance for industry, US Department of Health and Human Services. Food Drug Adm Cent Drug Eval Res CDER Cent Vet Med CVM Biopharm 1–44

40. Use C for MP for H (2018) Draft guideline on quality and equivalence of topical products. Eur. Med. Agency

41. World Health Organization. Regional Office for the Eastern Mediterranean (2008) List of basic sources in English for a medical faculty library. 117

42. (2006) Basic criteria for the in vitro assessment of dermal absorption of cosmetic ingredients, updated March 2006. 12

43. USEPA (2004) In vitro dermal absorption rate testing of certain chemicals of interest to the occupational safety and health administration; final rule. Fed Regist 69:22402–22441

44. Marks R, Leveque J-L, Voegeli R (2002) The Essential Stratum Corneum. https://doi.org/10.1201/b14296

45. Netzlaff F, Lehr C-M, Wertz PW, Schaefer UF (2005) The human epidermis models EpiSkin®, SkinEthic® and EpiDerm®: An evaluation of morphology and their suitability for testing phototoxicity, irritancy, corrosivity, and substance transport. Eur J Pharm Biopharm 60:167–178

46. Schäfer-Korting M, Bock U, Diembeck W, et al (2008) The Use of Reconstructed Human Epidermis for Skin Absorption Testing: Results of the Validation Study. Altern Lab Anim 36:161–187

47. Küchler S, Strüver K, Friess W (2013) Reconstructed skin models as emerging tools for drug absorption studies. Expert Opin Drug Metab Toxicol 9:1255–1263

48. Srinivasan M, Sedmak D, Jewell S (2002) Effect of fixatives and tissue processing on the content and integrity of nucleic acids. Am J Pathol 161:1961–1971

49. Lieber CA, Mahadevan-Jansen A (2003) Automated Method for Subtraction of Fluorescence from Biological Raman Spectra. Appl Spectrosc 57:1363–1367

50. Dancik Y, Kichou H, Eklouh-Molinier C, Soucé M, Munnier E, Chourpa I, Bonnier F (2020) Freezing Weakens the Barrier Function of Reconstructed Human Epidermis as Evidenced by Raman Spectroscopy and Percutaneous Permeation. Pharmaceutics 12:1041

51. Dancik Y, Jepps OG, Roberts MS (2007) 12 Beyond Stratum Corneum. Dermal Absorpt Toxic Assess 177:209

52. Zillich OV, Schweiggert-Weisz U, Hasenkopf K, Eisner P, Kerscher M (2013) Release and *in vitro* skin permeation of polyphenols from cosmetic emulsions. Int J Cosmet Sci 35:491–501

53. Tfayli A, Piot O, Draux F, Pitre F, Manfait M (2007) Molecular characterization of reconstructed skin model by Raman microspectroscopy: Comparison with excised human skin. Biopolymers 87:261–274

54. Tfaili S, Gobinet C, Josse G, Angiboust J-F, Manfait M, Piot O (2012) Confocal Raman microspectroscopy for skin characterization: a comparative study between human skin and pig skin. The Analyst 137:3673–3682

55. Guillard E, Tfayli A, Manfait M, Baillet-Guffroy A (2011) Thermal dependence of Raman descriptors of ceramides. Part II: effect of chains lengths and head group structures. Anal Bioanal Chem 399:1201–1213

56. Tfayli A, Guillard E, Manfait M, Baillet-Guffroy A (2010) Thermal dependence of Raman descriptors of ceramides. Part I: effect of double bonds in hydrocarbon chains. Anal Bioanal Chem 397:1281–1296

57. Frushour BG, Koenig JL (1975) Raman scattering of collagen, gelatin, and elastin. Biopolym Orig Res Biomol 14:379–391

58. Ali SM (2021) In vivo confocal Raman spectroscopic imaging of the human skin extracellular matrix degradation due to accumulated intrinsic and extrinsic aging. Photodermatol Photoimmunol Photomed 37:140–152

59. Resta V, Quarta G, Lomascolo M, Maruccio L, Calcagnile L (2015) Raman and Photoluminescence spectroscopy of polycarbonate matrices irradiated with different energy 28Si+ ions. Vacuum 116:82–89

60. Caetano L de VN, de Oliveira Mendes T, Bagatin E, Miot HA, Soares JLM, Martin AA (2017) In vivo confocal Raman spectroscopy for intrinsic aging and photoaging assessment. J Dermatol Sci 88:199–206

61. Stuart BH (1996) Temperature studies of polycarbonate using Fourier transform Raman spectroscopy. Polym Bull 36:341–346

62. Rodrigues F, Alves AC, Nunes C, Sarmento B, Amaral MH, Reis S, Oliveira MBP (2016) Permeation of topically applied caffeine from a food by—product in cosmetic formulations: Is nanoscale in vitro approach an option? Int J Pharm 513:496–503

63. OECD (2011) Guidance Notes on Dermal Absorption, Series on Testing and Assessment No. 156. OECD 36:1–72

64. Pulsoni I, Lubda M, Aiello M, Fedi A, Marzagalli M, von Hagen J, Scaglione S (2022) Comparison Between Franz Diffusion Cell and a novel Micro-physiological System for In Vitro Penetration Assay Using Different Skin Models. SLAS Technol.

65. Monteiro-Riviere NA, Inman AO, Zhang LW (2009) Limitations and relative utility of screening assays to assess engineered nanoparticle toxicity in a human cell line. Toxicol Appl Pharmacol 234:222–235

66. Bravo D, Rigley TH, Gibran N, Strong DM, Newman-Gage H (2000) Effect of storage and preservation methods on viability in transplantable human skin allografts. Burns 26:367–378

67. Barbero AM, Frasch HF (2016) Effect of frozen human epidermis storage duration and cryoprotectant on barrier function using two model compounds. Skin Pharmacol Physiol 29:31–40

68. Swarbrick J, Lee G, Brom J (1982) Drug permeation through human skin: I. Effects of storage conditions of skin. J Invest Dermatol 78:63–66

69. Dennerlein K, Schneider D, Göen T, Schaller KH, Drexler H, Korinth G (2013) Studies on percutaneous penetration of chemicals–impact of storage conditions for excised human skin. Toxicol In Vitro 27:708–713

70. Nielsen JB, Plasencia I, Sørensen JA, Bagatolli LA (2011) Storage conditions of skin affect tissue structure and subsequent in vitro percutaneous penetration. Skin Pharmacol Physiol 24:93–102

71. Payne OJ, Graham SJ, Dalton CH, Spencer PM, Mansson R, Jenner J, Azeke J, Braue E (2013) The effects of sulfur mustard exposure and freezing on transdermal penetration of tritiated water through ex vivo pig skin. Toxicol In Vitro 27:79–83

72. Sintov AC, Greenberg I (2014) Comparative percutaneous permeation study using caffeine-loaded microemulsion showing low reliability of the frozen/thawed skin models. Int J Pharm 471:516–524

73. Abdayem R, Roussel L, Zaman N, Pirot F, Gilbert E, Haftek M (2015) Deleterious effects of skin freezing contribute to variable outcomes of the predictive drug permeation studies using hydrophilic molecules. Exp Dermatol 24:972–974

74. Kemppainen BW, Riley RT, Pace JG, Hoerr FJ (1986) Effects of skin storage conditions and concentration of applied dose on [3H] T-2 toxin penetration through excised human and monkey skin. Food Chem Toxicol 24:221–227

75. Sintov AC (2017) Cumulative evidence of the low reliability of frozen/thawed pig skin as a model for in vitro percutaneous permeation testing. Eur J Pharm Sci 102:261–263

76. Morin M, Runnsjö A, Ruzgas T, Engblom J, Björklund S (2023) Effects of storage conditions on permeability and electrical impedance properties of the skin barrier. Int J Pharm 637:122891

77. Planz V, Lehr C-M, Windbergs M (2016) In vitro models for evaluating safety and efficacy of novel technologies for skin drug delivery. J Controlled Release 242:89–104

78. Stefanakis M, Bassler MC, Walczuch TR, Gerhard-Hartmann E, Youssef A, Scherzad A, Stöth MB, Ostertag E, Hagen R, Steinke MR (2023) The Impact of Tissue Preparation on Salivary Gland Tumors Investigated by Fourier-Transform Infrared Microspectroscopy. J Clin Med 12:569

79. Ge L, Huang Z, Wei H (2011) Skin graft preservation. Skin Grafts-Indic. Appl. Curr. Res.

80. Verbeken G, Verween G, De Vos D, Pascual B, De Corte P, Richters C, De Coninck A, Roseeuw D, Ectors N, Rose T (2012) Glycerol treatment as recovery procedure for cryopreserved human skin allografts positive for bacteria and fungi. Cell Tissue Bank 13:1–7

81. Petrilli R, Eloy JO, Praça FSG, Del Ciampo JO, Fantini MAC, Fonseca MJV, Bentley M (2016) Liquid crystalline nanodispersions functionalized with cell-penetrating peptides for topical delivery of short-interfering RNAs: a proposal for silencing a pro-inflammatory cytokine in cutaneous diseases. J Biomed Nanotechnol 12:1063–1075

82. Estracanholli ÉA, Praça FSG, Cintra AB, Pierre MBR, Lara MG (2014) Liquid crystalline systems for transdermal delivery of celecoxib: in vitro drug release and skin permeation studies. Aaps Pharmscitech 15:1468–1475

83. Barbero AM, Frasch HF (2009) Pig and guinea pig skin as surrogates for human in vitro penetration studies: a quantitative review. Toxicol In Vitro 23:1–13

84. Meade AD, Clarke C, Draux F, Sockalingum GD, Manfait M, Lyng FM, Byrne HJ (2010) Studies of chemical fixation effects in human cell lines using Raman microspectroscopy. Anal Bioanal Chem 396:1781–1791

85. Faolain EO, Hunter MB, Byrne JM, Kelehan P, McNamara M, Byrne HJ, Lyng FM (2005) A study examining the effects of tissue processing on human tissue sections using vibrational spectroscopy. Vib Spectrosc 38:121–127

86. Bakar J, Michael-Jubeli R, Tfaili S, Assi A, Baillet-Guffroy A, Tfayli A (2021) Biomolecular modifications during keratinocyte differentiation: Raman spectroscopy and chromatographic techniques. The Analyst 146:2965–2973

87. Tfayli A, Guillard E, Manfait M, Baillet-Guffroy A (2012) Raman spectroscopy: feasibility of in vivo survey of stratum corneum lipids, effect of natural aging. Eur J Dermatol EJD 22:36–41

88. Choe C, Schleusener J, Lademann J, Darvin ME (2017) In vivo confocal Raman microscopic determination of depth profiles of the stratum corneum lipid organization influenced by application of various oils. J Dermatol Sci 87:183–191

89. Choe C, Schleusener J, Lademann J, Darvin ME (2018) Age related depth profiles of human Stratum Corneum barrier-related molecular parameters by confocal Raman microscopy in vivo. Mech Ageing Dev 172:6–12